

Supporting Information

Advanced Continuous-Flow Microfluidic Device for Parallel Screening of Crystal Polymorphs, Morphology and Kinetics at Controlled Supersaturation

Paria Coliaie¹, Manish S. Kelkar², Marianne Langston³, Chengxiang Liu⁴, Neda Nazemifard⁵, Daniel Patience⁴, Dimitri Skliar⁶, Nandkishor K. Nere^{1,2}, and Meenesh R. Singh^{1,*}

¹Department of Chemical Engineering, University of Illinois at Chicago, Chicago, IL 60607

²Center of Excellence for Isolation & Separation Technologies (CoExIST), Process R&D, AbbVie Inc., North Chicago, IL 60064

³Pharmaceuticals Research – Analytical Development, Takeda Pharmaceuticals International Co., Cambridge, MA 02139

⁴Pharmaceutical Development, Biogen, Cambridge, MA 02142

⁵Chemical Process Development, Takeda Pharmaceuticals International Co., Cambridge, MA 02139

⁶Chemical Process Development, Product Development, Bristol Myers Squibb Co., New Brunswick, NJ 08901

Corresponding Author Email: mrsingh@uic.edu

Table of Contents

<i>S1. Merged-Inlet Microfluidic Device: Design, Dimension and Fabrication</i>	3
S1.1 Design of the Merged-Inlet Microfluidic Device	3
S1.2 Dimensions of the Microfluidic Device: Merged-Inlet Single-Well and the Array of the Merged-Inlets	3
S1.3 Fabrication of the Microfluidic Device: Merged-Inlet Single-Well and the Array of the Merged-Inlets	5
<i>S2. COMSOL Simulation of the Merged-Inlet Microfluidic Device</i>	6
S2.1 Laminar Flow Module: Equations and Boundary Conditions	6
S2.2 Transport of Diluted Species Module: Equations and Boundary Conditions	6
S2.3 Model Parameters of the Simulations	7
S2.4 Hydrodynamic Performance Analysis	8
S2.5 Grid Dependency Analysis: Pressure and Concentration Profile.....	11
S2.6 Reliability Analysis: Pressure and Concentration Profile	13
<i>S3. Details of Experimental Condition for Each Well in the Multi-Well.....</i>	13
<i>S4. Calculation of the Residence Time Distribution.....</i>	15
<i>S5. Solubility Measurements of Form A Of L-Histidine in Different Ratios of Ethanol and Water at Room Temperature Using Separated Inlets Microfluidic Mixer</i>	15
<i>S6. Polymorphs Face Detection for Growth Rate Measurements and Sample of Growth Rate Measurement</i>	17
<i>S7. X-Ray Diffraction Patterns of L-Histidine Polymorphs</i>	19
<i>S8. Temperature Control Strategy for the Merged-Inlet Single-Well Device.....</i>	23
<i>S9. Increasing the Throughput of the Merged-Inlet Microfluidic Mixer.....</i>	23

S1. Merged-Inlet Microfluidic Device: Design, Dimension and Fabrication

S1.1 Design of the Merged-Inlet Microfluidic Device

In Figure 1A of the manuscript, we have shown the 3D design of a multi-inlet single-well microfluidic device. The arrangement of inlets in this design will not allow multiple wells to be accommodated on a single block. To address this issue, we have introduced a merged-inlet single-well design shown in Figure 1B. In the merged-inlet design, the four tangential channels connected to the cylindrical zone are intact. However, the two non-neighboring inlets are combined and merged into a single major inlet. Repeating this for the other two channels, the total number of major inlets that appear on the side of the device will decrease from four to two. The new arrangement of the inlets on the side allows for accommodating several wells next to each other. As shown in Figure 1B (Internal view), the two merged connections are lifted upward and downward of the plane that the four tangential inlets are connected to the cylindrical zone. This shift is necessary to avoid the intersection of channels and does not affect the performance of the device. For more clarification, the 3D design of the merged-inlet single-well device is provided in a ESI movie file.

S1.2 Dimensions of the Microfluidic Device: Merged-Inlet Single-Well and the Array of the Merged-Inlets

In Figure S1, top, isometric and side views of the merged-inlet single-well are shown. The required dimensions for drawing the merged-inlet single-well device are provided in Table S1.

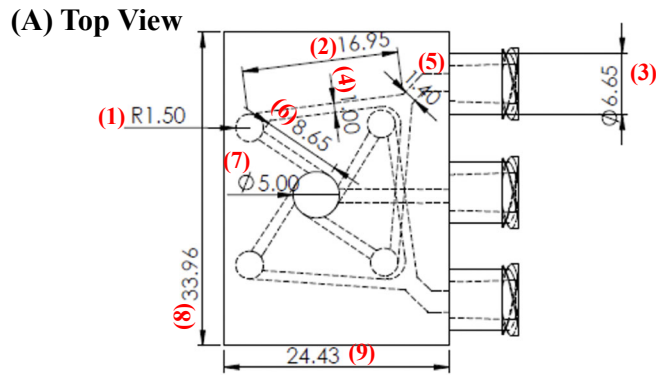


Table S1: Dimensions Of The Merged-inlet Single Well

Dimension	Value (mm)
1	1.5
2	16.95
3	6.65
4	1
5	1.4
6	8.65
7	5
8	33.96
9	24.43
10	9
11	1
12	2.5
13	1
14	1.5
15	1
16	9
17	1
18	1

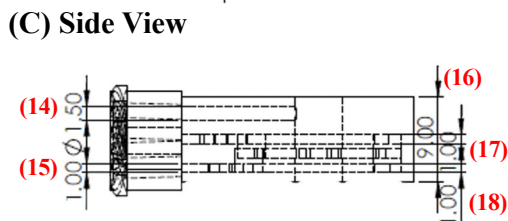
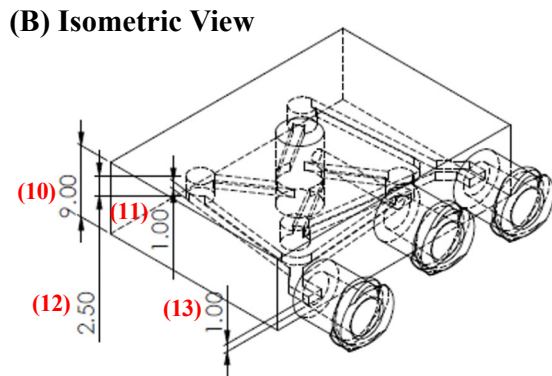


Figure S1: (A) Top view, (B) Isometric view, (C) Side view of the merged-inlet single well with dimensions marked

This design is repeated eight times for designing the array of the merged-inlet wells, as shown in Figure 1C. In Figure S2, we have demonstrated the dimension of the array of the merged-inlet wells.

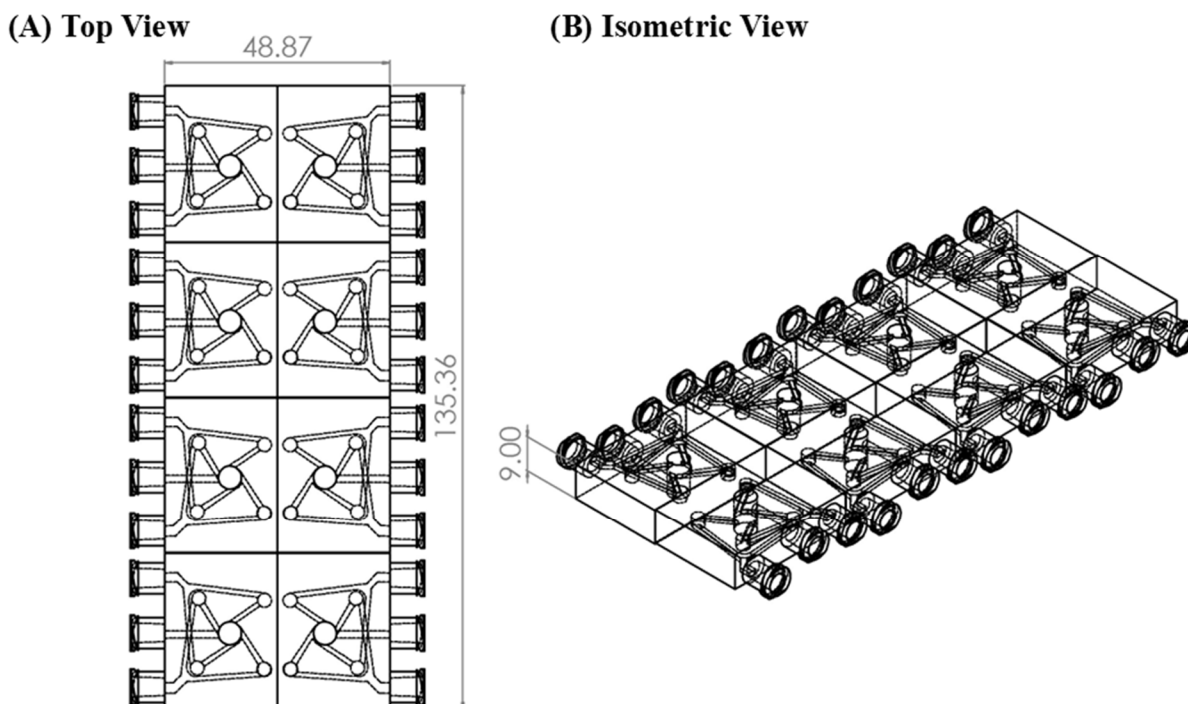


Figure S2: (A) Top view, and (B) Isometric view of the array of the merged-inlet wells with marked dimensions.

S1.3 Fabrication of the Microfluidic Device: Merged-Inlet Single-Well and the Array of the Merged-Inlets

All the microfluidic devices were fabricated using stereolithography (SLA) 3D printing technology. We first prepared the CAD design using 3D designing software. Here we have used SolidWorks® (2018, Dassault Systems) to prepare the CAD design of the single well and array of the merged-inlet wells. (shown in Figure S2). We have then used a commercial 3D printer (form 2, Formlabs Inc., USA) to print the devices. The selected resin for the prints was the clear resin which is chemically resistant to various solvents, including ethanol and water. After printing the device, they are washed in an isopropyl alcohol (IPA) (90%, Sigma-Aldrich) bath for 20 mins in the Form Wash (Formlabs Inc., USA) to remove the residues of the resin from the external surface. The interior channels of the 3D printed device were washed separately by injecting IPA using a syringe to eliminate the uncured residues of the resin in the channels.

As shown in Figure 2B in the manuscript, the top and bottom faces of the microfluidic mixer were kept open to maximize optical clarity. The open holes on both sides were sealed with polycarbonate films using a fresh, clear resin. First, the area around the circular zone is covered with fresh uncured resin (from the resin tank), and a polycarbonate film is put on that. Next, the device is cured under UV light for 10 minutes to seal the open area. Figure S3 shows the step-by-step procedure for sealing the open holes of the 3D printed device.

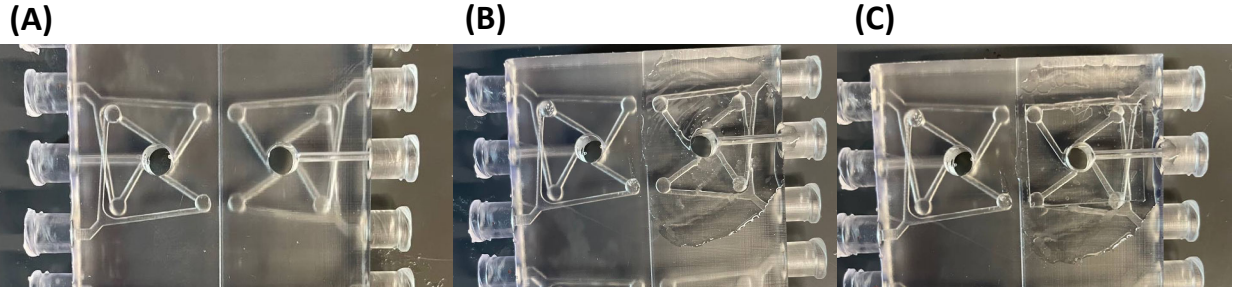


Figure S3: Sealing procedure for the merged-inlet microfluidic, (A) Open holes on both sides, (B) fresh resin on the surface, (C) polycarbonate film covering the open hole.

S2. COMSOL Simulation of the Merged-Inlet Microfluidic Device

S2.1 Laminar Flow Module: Equations and Boundary Conditions

The laminar flow module of COMSOL was used to calculate the velocity profile in the microfluidic mixer. The time-dependent Navier Stock equation solved is described as follows:

$$\rho \frac{\partial u}{\partial t} + \rho(u \cdot \nabla)u = \nabla \cdot [-p \cdot I + \mu(\nabla u + (\nabla u)^T)] + F \quad \text{Eq (1)}$$

In Eq (1), the density and the viscosity are defined for the mixture of ethanol and water. The fluid is assumed to be incompressible, and the temperature is constant and equal to 298.15 K for all the simulations. The assigned boundary conditions are listed below and shown in Figure S4:

Boundary Conditions:

- Inlet 1: $Q = 0.5 \text{ mL} \cdot \text{min}^{-1}$
- Inlet 2: $Q = 0.5 \text{ mL} \cdot \text{min}^{-1}$
- Outlet: $P = 1 \text{ atm}$

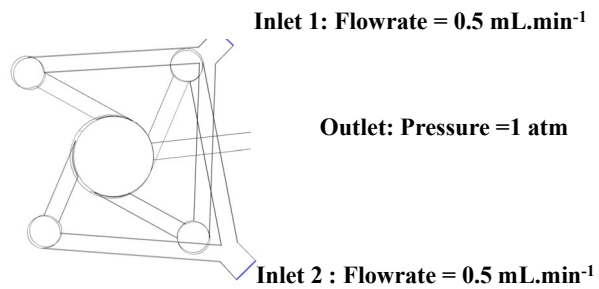


Figure S4: The top view of the merged inlet microfluidic mixer design with the assigned boundary conditions for the two inlets and one outlet in the laminar flow module

S2.2 Transport of Diluted Species Module: Equations and Boundary Conditions

The transport of the diluted species module is used to calculate the concentration profile in the microfluidic mixer. The time-dependent continuity equation solved is described as follows:

$$\rho \frac{\partial c_i}{\partial t} + \nabla \cdot (-D_i \nabla c_i) + u \cdot \nabla c_i = R_i \quad \text{Eq(2)}$$

which includes both convection and diffusion for the transport mechanisms. Here ρ is the density and u is the velocity of the fluid and comes from the laminar flow module. These two modules are coupled together, and the velocity profile is directly substituted into the continuity equation. The assigned boundary conditions for this model are listed below and shown in Figure S5:

Boundary Conditions:

- Inlet 1: $c_i = c_{0,i} = 0 \text{ mol. m}^{-3}$
- Inlet 2: $c_i = c_{0,i} = 1 \text{ mol. m}^{-3}$
- Outlet: $n \cdot D_i \nabla c_i = 0$

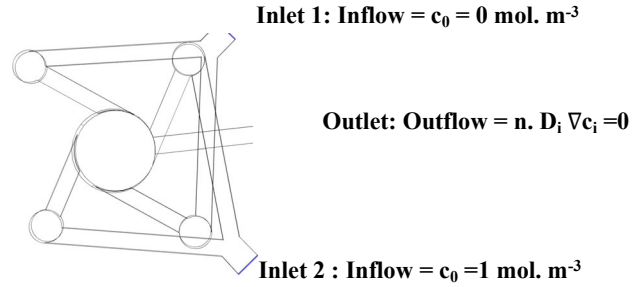


Figure S5: The top view of the merged inlet microfluidic mixer design with the assigned boundary conditions for the two inlets and one outlet in the transport of the diluted species module

S2.3 Model Parameters of the Simulations

In this study, we have simulated a coupled analysis of the laminar flow module and transport of the diluted species to evaluate the velocity pressure and concentration profile inside the microfluidic mixer. The 3D model for simulations was imported into the model from a Solid Work design. The design was further simplified by eliminating the sharp edges and smoothening the surfaces to enhance the mesh quality. The free tetrahedral mesh was selected for the models. The tetrahedral mesh was selected for this study, and the details are provided in the following part:

- Maximum Element Size = 2.07 mm
- Minimum Element Size = 0.518 mm
- Maximum Element Growth Rate = 1.3
- Curvature Factor = 0.9
- Resolution of Narrow Region = 0.4

For the corner refinements, the settings were set to the following values:

- Minimum Angle Between Boundries = 240
- Element Size Scaling Factor = 0.35

For the boundary layer, the settings were set to the following values:

- Handling of Sharp Edges = Trimming

- Minimum Angle for Trimming = 240
- Maximum Angle for Trimming = 50
- Maximum Layer Decrement = 2
- Number of Iteration = 4
- Maximum Element Depth to Process = 6

The coupled equations of the Navier stock and mass balance were solved in the stationary solver using linear solver “Algebraic Multigrid” (GMRES). The residual tolerance was set to 0.01 with 200 iterations and left preconditioning. Newton was selected as the non-linear method with a damping factor of 0.1 and tolerance as the termination technique. The relative tolerance was also kept at 0.001. The concentration-dependent viscosity and density of the water-ethanol mixture at room temperature were considered in the model.

The boundary condition for the rest of the boundaries was set to wall condition = no-slip boundary condition. ($u = 0$)

S2.4 Hydrodynamic Performance Analysis

As shown in Figure 1B (Internal view), the merged inlet connections are shifted up and down from the plane of the four tangential inlets. Each inlet has an equal distance for end-to-end to ensure that the pressure drop in all four inlets is identical. The pressure drop is an important factor as the change in the pressure drop will change the velocity distribution. The effect of Y-junction in the merged-inlet single-well design on pressure drops difference between four tangential inlets is evaluated using computational fluid dynamics (CFD) simulation. Also, its effect on the velocity profile in each inlet and mixing in the micromixer is evaluated computationally.

- **Distance from the main inlet:** In Figure 3B, we have shown the gauge pressure in mPa for each channel versus the distance from the main inlet. The distance from the main inlet is measured as shown in Figure S6 below:

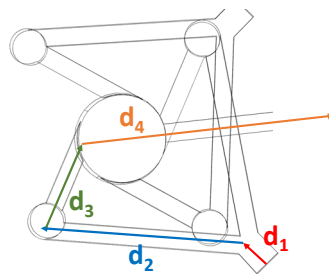


Figure S6: Top view of the merged-inlet single well with four arrows indicating the distance from the main inlets.

Since all the dimensions were kept identical for both major inlets, this distance is equal for all four tangential inlets.

$$\text{Distance from the main inlet} = d_1 + d_2 + d_3 + d_4 \quad \text{Eq(3)}$$

- **Contour Pressure Profile for the Merged-Inlet Single-Well:** In addition to the pressure drop comparison shown in Figure 3B of the main article, we have shown the pressure contour for the merged-inlet single-well microfluidic device. Figure S7 shows the isometric view and top view of the pressure contours and confirms the identical pressure difference in all four inlets.

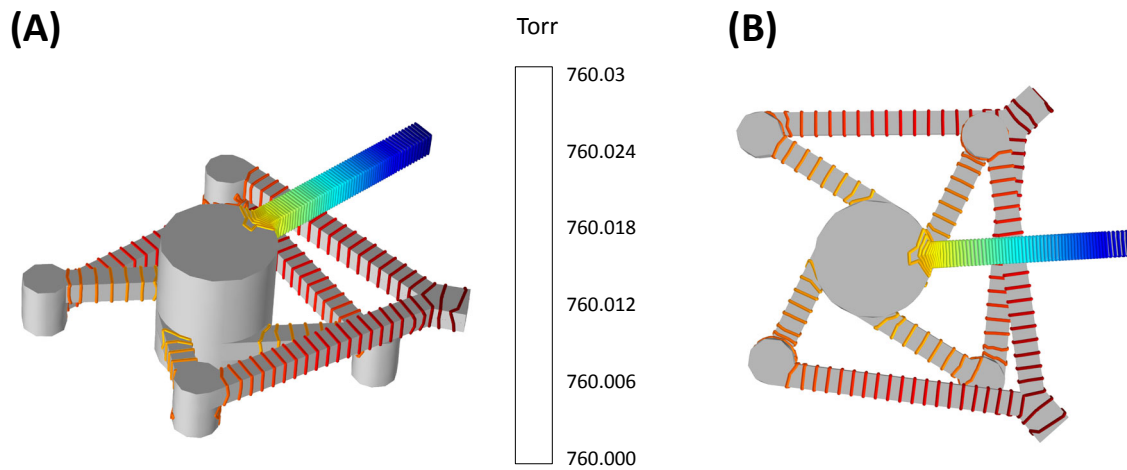


Figure S7: Contour pressure profile of the merged-inlet single-well microfluidic device (A) Isometric view; (B) Top view

- **Velocity Profile for the Merged-Inlet Single-Well:** In addition to the pressure profile, we have also computed and plotted the velocity profile of the merged-inlet single-well microfluidic mixer. Figure S8 shows that the velocity profile inside the merged-inlet single-well microfluidic device is identical, which confirms that the flow distribution is not affected by the merging of inlets using Y-junctions

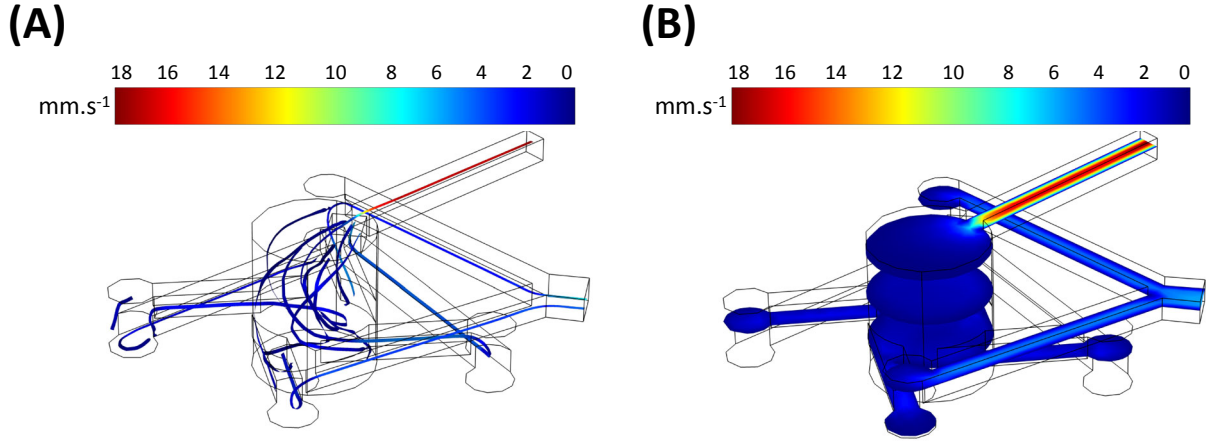


Figure S8: Velocity profile in the merged-inlet single-well microfluidic device (A) Streamlines inside the channels and mixer; (B) Average velocity at different vertical slices in the device.

- **Evaluation of the Mixing Index:** The mixing index is used in this study to evaluate the performance of the mixing in the merged-inlet single-well microfluidic device. The height of the mixer is divided into 20 parallel planes to calculate the mixing index. In each plane, the concentration profile was obtained from COMSOL, and then data was exported and post-processed in MATLAB. Next, the standard deviation of the concentration in each plane is calculated to obtain Mixing Index as follows:

$$Mixing\ Index = 1 - \left(\frac{\sigma^2}{\sigma_0^2} \right) \quad Eq(4)$$

where σ_0^2 is the concentration variance of the bottom plane and σ^2 in any plane above the bottom plane. From Eq (4), the mixing index for each plane was calculated. For $z = 0$, the mixing index is equal to 0 as σ_0^2 and σ^2 are same. As we move upward, the variance of the concentration decreases, and hence mixing index increases. A sample of calculation for the mixing index is shown in Table S2.

Table S2: Calculated Mixing Index for the Merged-Inlet Single-Well Microfluidic Device

Z (mm)	Standard Deviation	Variance	Mixing Index
0	0.325	0.105	0
1	0.27	0.073	0.31
1.5	0.179	0.032	0.7
2	0.105	0.011	0.89
2.5	0.064	0.004	0.96
3	0.04	0.002	0.98
3.5	0.026	0.001	0.99
4	0.016	0	1
4.5	0.01	0	1
5	0.007	0	1
5.5	0.0004	0	1
6	0.0004	0	1
6.5	0.0004	0	1
7	0.0004	0	1
7.5	0.0004	0	1
8	0.0004	0	1
8.5	0.0004	0	1
9	0.0004	0	1

S2.5 Grid Dependency Analysis: Pressure and Concentration Profile

To investigate the effect of the grid size on the result of the simulation, we have simulated continuity equation for concentration profile and Navier Stokes equation for pressure and velocity profile for the merged-inlet single-well design for six different grid sizes, while keeping all other solver configurations (given in Section 2.2 of the main article) same.

- *Grid 1 = Normal Refined;*
- *Grid 2 = Normal;*
- *Grid 3 = Coarse;*
- *Grid 4 = Coarser;*
- *Grid 5 = Extra Coarse;*
- *Grid 6 = Extremely Coarse;*

In Table S3, the detail of each grid is provided.

Table S3: Details of the six different grids used for the Grid Dependency Analysis

	Max Element Size (mm)	Min Element Size (mm)	Max Element Growth Rate	Curvature Factor	Resolution of Narrow Regions
Normal Refined	0.694	0.207	1.15	0.6	0.7
Normal	0.694	0.207	1.15	0.6	0.7
Coarse	1.04	0.311	1.2	0.7	0.6
Coarser	1.35	0.414	1.25	0.8	0.5
Extra Coarse	2.07	0.518	1.3	0.9	0.4
Extremely Coarse	3.42	0.725	1.4	1	0.3

* *The normal refined grid is created by making a single refinement on the normal grid using "split the longest side" method.*

The calculated standard deviation (SD) for four planes in each simulation is listed in Table S3. The 3rd plane with a 2 mm distance from the inlets is then selected for comparing the mixing index in the five simulations. Additionally, the maximum pressure drop between the inlet and outlet ($d_1+d_2+d_3+d_4$) is calculated for every grid size. In Table S4, we have shown the calculated values of the mixing indices for different grids and the maximum pressure drop between inlet and outlet. SD is the standard deviation in the selected plane, which is used to calculate the mixing index. (see section S2.4 in the ESI for the details of the calculation of the mixing index)

The mixing index and pressure drop data are also plotted vs. the grid size in Figure S9. Figure S9 shows the results of these simulations are independent of the grid size. The mixing index at $z=2$ mm is between 0.88 to 0.91 for all six tested grid sizes. The maximum pressure difference also is between 3.5 to 3.7 Pa for all the tested grid sizes.

Table S4: Calculated values of mixing indices and maximum pressure drop between inlet and outlet for different grid size

	Normal Refined	Normal	Coarse	Coarser	Extra Coarse	Extremely Coarse
SD (Z=0 mm)	0.2835	0.34	0.29	0.33	0.32	0.32
SD (Z=1 mm)	0.2107	0.26	0.25	0.25	0.24	0.25
SD (Z=2 mm)	0.0878	0.11	0.11	0.09	0.1	0.11
SD (Z=3mm)	0.0609	0.07	0.07	0.06	0.06	0.07
SD²(Z=0 mm)	0.08	0.11	0.08	0.11	0.11	0.1
SD²(Z=2 mm)	0.01	0.01	0.01	0.01	0.01	0.01
Mixing Index (Z=2)	0.9	0.9	0.85	0.92	0.91	0.88
Max Pressure Drop (Pa)	3.7	3.5	3.7	3.6	3.7	3.7

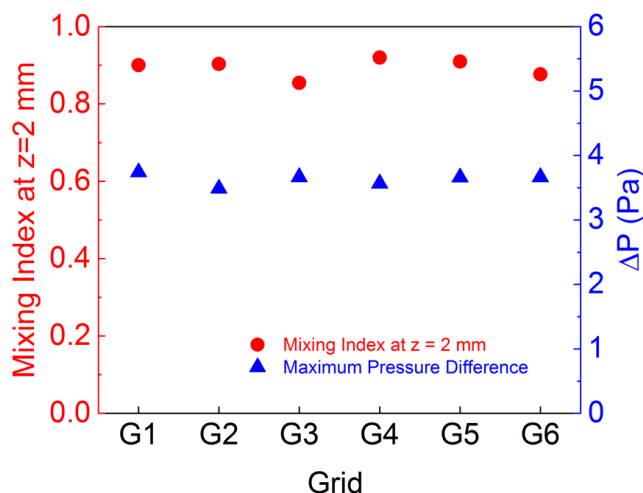


Figure S9: Mixing index and maximum pressure drop for the six different grids

S2.6 Reliability Analysis: Pressure and Concentration Profile

We have performed simulations for three different relative tolerance while keeping all other solver parameters constant. The reliability of the simulations can be confirmed from the variation in maximum pressure drop and the mixing index with respect to relative tolerances. As shown in Table 5, there is no change in the maximum pressure drop and the mixing index for different relative tolerances. This confirms that the simulation results are reliable within the chosen range of relative tolerances.

Table S5: Effect of relative tolerance on the maximum pressure drop and mixing index

Relative Tolerance	Max Pressure Drop	Mixing Index
1.00E-01	3.48	0.91
1.00E-03	3.48	0.91
1.00E-05	3.48	0.91

S3. Details of Experimental Condition for Each Well in the Multi-Well

Figure S10 shows a schematic of an array of the merged inlets with the assigned experimental conditions. In Table S6, flowrates, L-Histidine concentration, and the solubility of L-Histidine at each ratio of ethanol and water are provided.

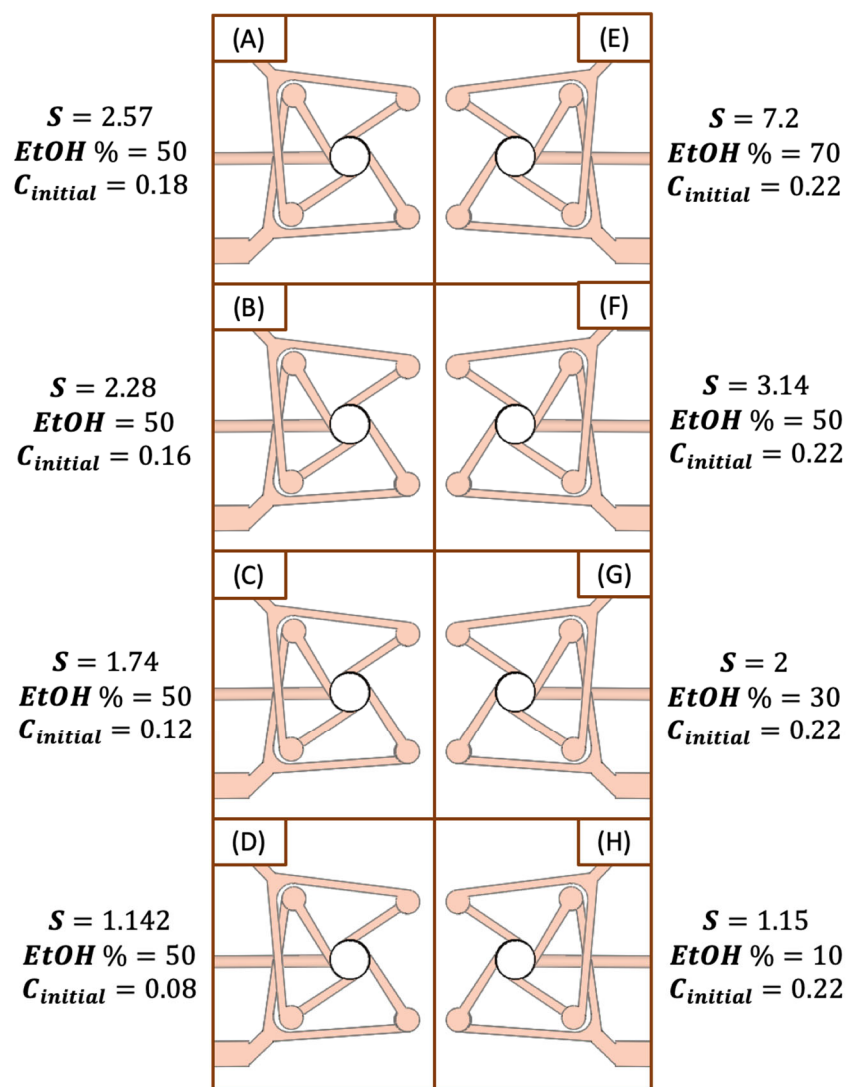


Figure S10: Array of the merged inlets with marked experimental conditions

Table S6: Details of Experimental Condition for the Multi-Well Experiment

Samples	Feed Concentration	Ethanol Percentage (%)	Mixer Concentration	c^*	Supersaturation	L-Histidine Flowrate (ml/min)	Ethanol Flowrate
A	0.18	50	0.09	0.04	2.57	0.5	0.5
B	0.16	50	0.08	0.04	2.28	0.5	0.5
C	0.12	50	0.06	0.04	1.74	0.5	0.5
D	0.08	50	0.04	0.04	1.14	0.5	0.5
E	0.22	70	0.066	0.01	7.23	0.3	0.7
F	0.22	50	0.11	0.04	3.14	0.5	0.5
G	0.22	30	0.154	0.08	2	0.7	0.3
H	0.22	10	0.198	0.17	1.15	0.9	0.1

S4. Calculation of the Residence Time Distribution

In order to calculate the residence time distribution of the merged inlet microfluidic mixer, the concentration at the outlet is recorded from $t = 0$ to $t = 15$ minutes at each flowrate. The flow rate was varied from 0.1 to 1 with increments of $0.1(\frac{ml}{min})$. Using MATLAB, these data were processed to calculate the average residence time and standard deviation at each flowrate. The outlet concentration at different time $\bar{c}(t)$ is first divided by the initial concentration which is set as $1(\frac{ml}{min})$:

$$F(t) = \frac{\bar{c}(t)}{c_0} \quad \mathbf{Eq(5)}$$

Here $c(0)$ is the initial concentration and $\bar{c}(t)$ is the average concentration at the outlet boundary. From here, the average residence time \bar{t} and the standard deviation (σ) is calculated as:

$$\bar{t} = \int_0^{\infty} [1 - F(t)] dt \quad \mathbf{Eq(6)}$$

$$\sigma^2 = 2 \int_0^{\infty} t[1 - F(t)] dt - \bar{t}^2 \quad \mathbf{Eq(7)}$$

The values of \bar{t} and σ are calculated for each flowrate and the results are shown in Figure 3E.

S5. Solubility Measurements of Form A Of L-Histidine in Different Ratios of Ethanol and Water at Room Temperature Using Separated Inlets Microfluidic Mixer

In order to measure the solubility of form A of L-histidine in different ratios of ethanol and water, a saturated solution of L-histidine in the water at room temperature is prepared. The four entering streams into the microfluidic mixer include two streams of saturated solution, one stream of pure solvent (water), and one stream of pure antisolvent (ethanol). A schematic of the setup mentioned above is shown in Figure S11.

The flowrate of the ethanol (Q_3) is initially set to the desired ratio and then kept constant with respect to the summation of the flowrates for the solution of L-his in water (Q_1) and pure water (Q_2) After that, starting from the highest ratio of the pure solvent, Q_1 is increased and consequently Q_2 is decreased. However, the summation of Q_1 and Q_2 should remain constant. The point where crystals are formed within the microfluidic mixer is then considered the maximum point, and then the several ratios before that value are checked to obtain the values of the flowrates of all three streams and measure the solubility.

Knowing the concentration of the L-histidine in the water, solubility is calculated as following:

$$C_{eq} = \frac{c_{initial} \times Q_1}{Q_1 + Q_2 + Q_3} \quad Eq(8)$$

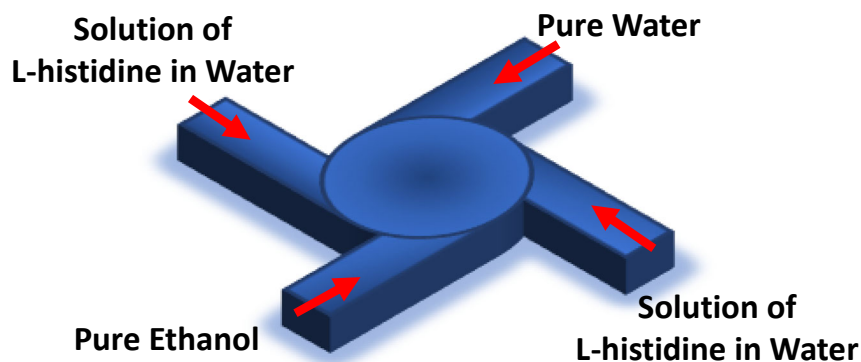


Figure S11: Schematic of entering streams into the microfluidic mixer for solubility measurement experiments

The time intervals selected to wait for equilibrium are 1, 3, 5, and 10 minutes. The solubility data have been calculated for each of these wait times and plotted in Figure S12. The results were compared with the solubility data of the L-histidine at different ratios of ethanol-water from the literature. The results show that the five minutes wait time results in the closest values to the literature.

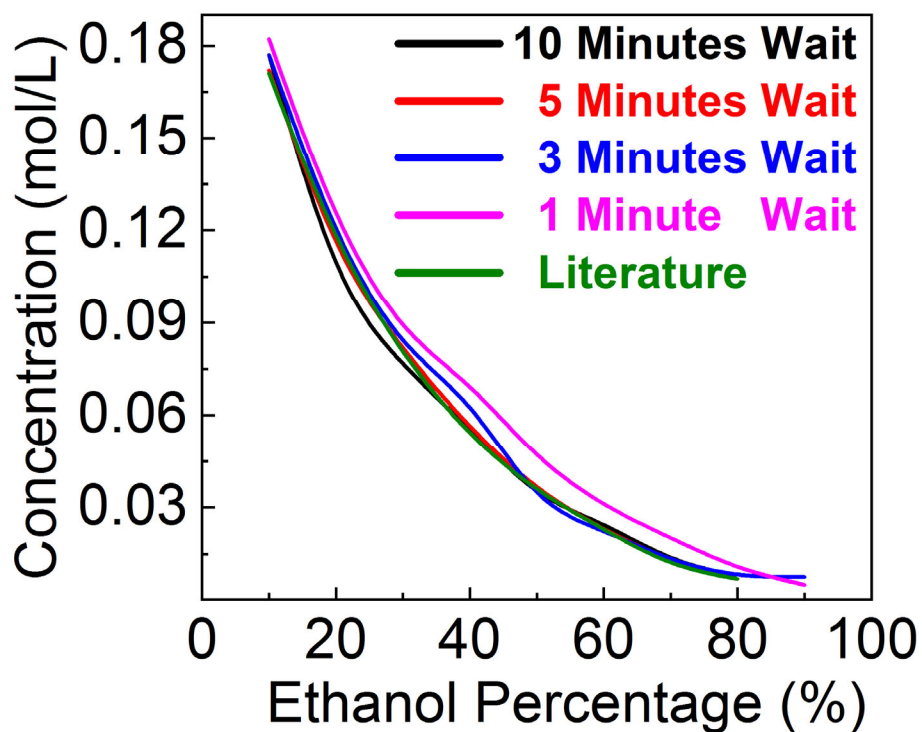


Figure S12: Solubility curve of form A of L-histidine at different ratios of ethanol-water obtained at different waiting times.

S6. Polymorphs Face Detection for Growth Rate Measurements and Sample of Growth Rate Measurement

Figure S13 shows the simulated crystals of form B from experimental samples. The detected faces from the XRD spectra were

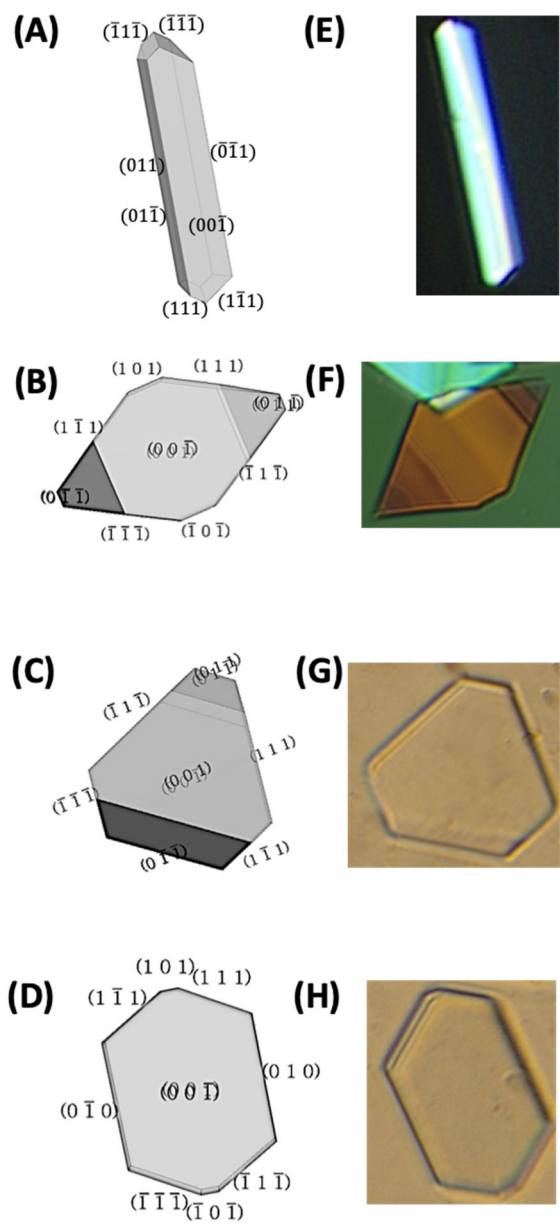


Figure S13: Crystal morphologies of form A and selected form B crystals of L-Histidine with shown faces: (A) Predicted morphology of form A. (B), (C) and (D) Predicted morphology of form B. (E) Optical image of the form A crystals obtained experimentally. (F), (G) and (H) Optical image of the form B crystals obtained experimentally.

Growth Rate Measurements:

The growth rate data were obtained by taking time-lapse images from samples every five minutes. The change in the distance from face 111 was divided by the time difference. Here we have shown a sample of these calculations. In Figure S14, we have shown five pictures taken in 20 minutes for sample B ($S=2.28$). Table S6 includes all the measurements and the growth rate measurements.

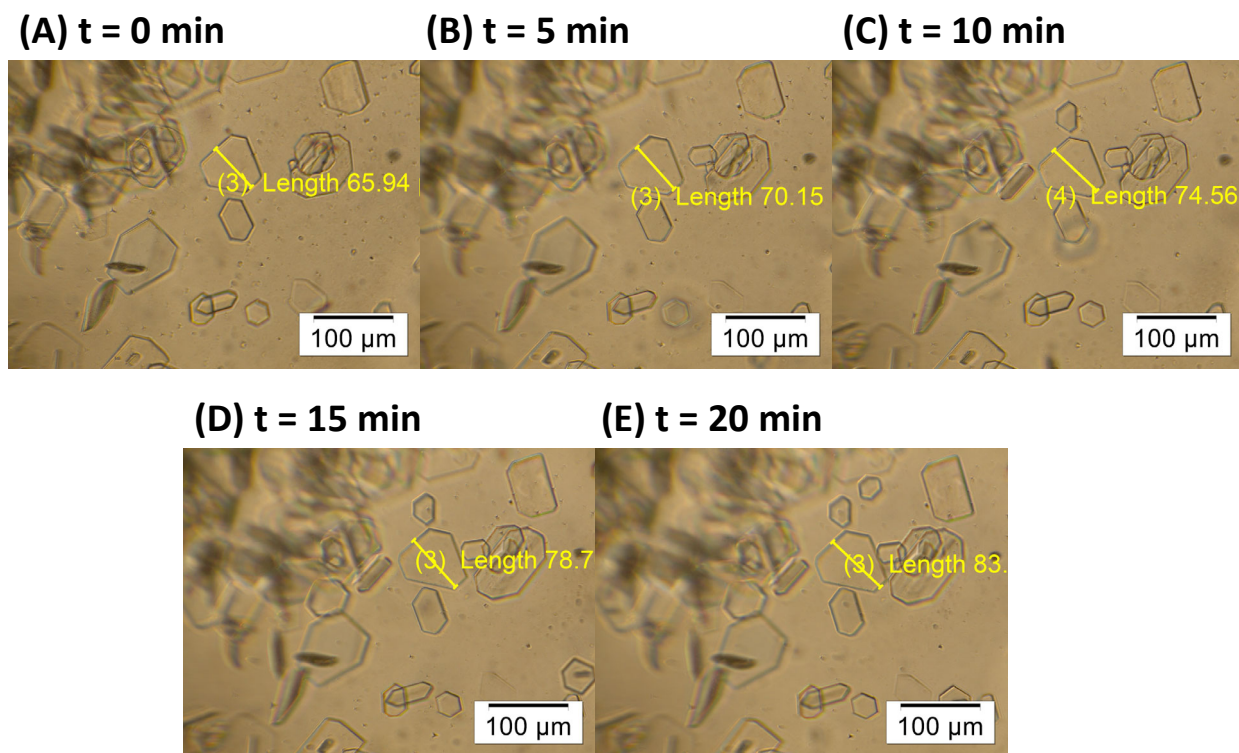


Figure S14: Time-lapse images from the sample B ($S=2.28$) for 20 minutes. The $t=0$ is not the initial time of the experiments, and it is the time when the measurements started.

Table S7: Growth rate measurements for sample B ($S=2.28$)

t = 0 min	t = 5 min	t = 10 min	t = 15 min	t = 20 min	Mean (Growth Rate[$\mu\text{m.s}^{-1}$])	Standard Deviatton (Growth Rate)
65.94	70.15	74.56	78.76	83.01		
0.1403	0.147	0.14	0.1417		0.01437	0.0004714

The unit for all the measurements in Table S7 and Figure S14 is μm . This procedure is repeated and the average growth rate for several crystals from each sample is reported.

S7. X-Ray Diffraction Patterns of L-Histidine Polymorphs

Figure S15 shows simulated and experimental XRD patterns for pure Form A and Form B. The XRD of Form A was taken directly for as-purchased L-Histidine (Sigma-Aldrich, chemical purity $\geq 99\%$). The pure form B was prepared by cooling crystallization of a saturated solution of L-Histidine at 70°C .

Based on the subplots in Figure S15, we can conclude that experimental spectra for both polymorphs match with the simulated spectra. In the simulated XRD spectra, all the possible facets of the crystals exposed during scanning are shown. However, in the experimental XRD pattern, only the facets that are preferentially oriented are exposed. Also, a slight shift in the experimental XRD spectra as compared to simulated spectra for sample A can be due to the specimen displacement. It is a systematic peak position error due to the misalignment of the sample.

In Figure S15, we have dashed vertical lines to show the slight shifts in the major peaks for the experimental XRD spectra of Form A.

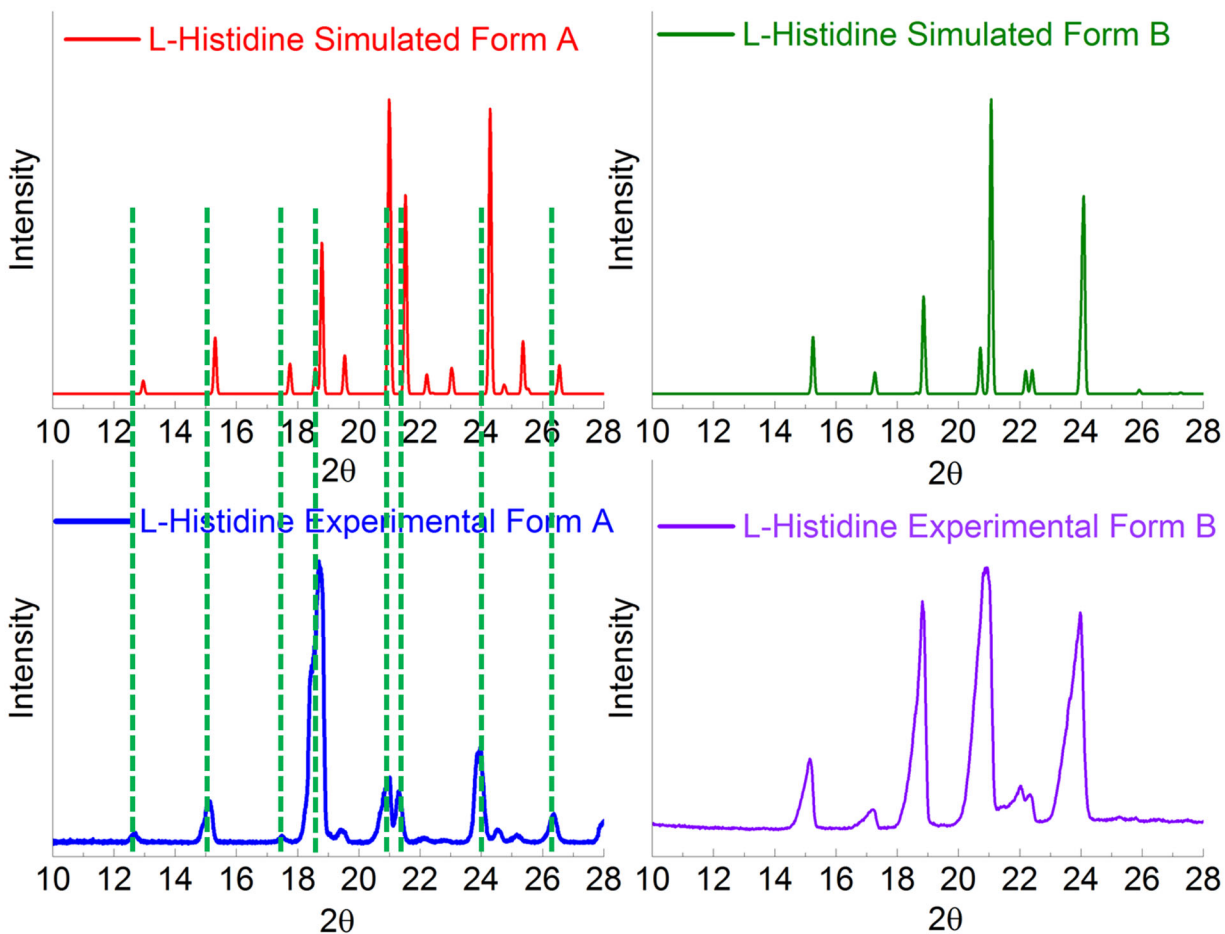


Figure S15: XRD patterns of L-Histidine polymorphs: (A) Simulated form A. (B) Simulated form B. (C) Experimental form A. (D) Experimental form B.

After confirming the pure Form of each polymorph, five mixtures of these pure forms were prepared with a total mass of 0.1 g. The total mass of the crystals was used in a 5 cm sample holder for obtaining the XRD spectra. In Figure S16, the spectra of these five samples, as well as pure forms, are shown in the order of increasing weight % of form B.

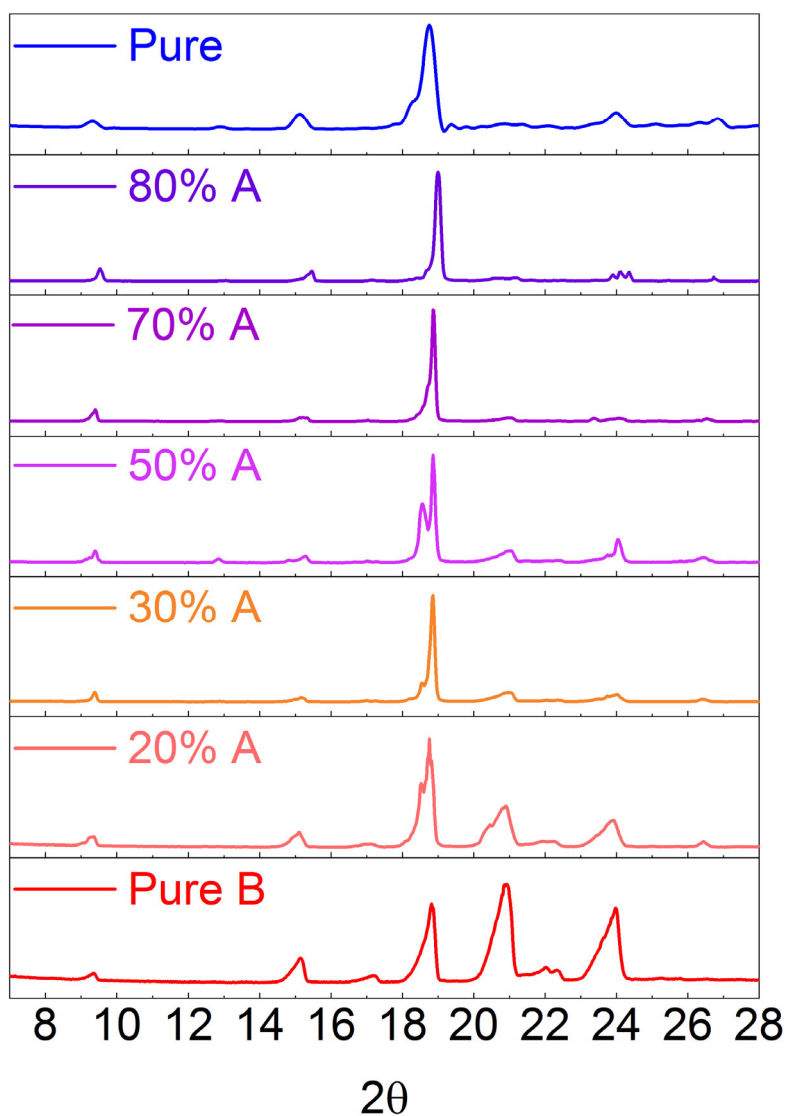


Figure S16: XRD spectra of mixtures of form A and B and their pure forms.

There are two distinct peaks shown in Figure S17; one appears in form B but does not exist in Form A (Figure S17, A). The second peak appears in Form A but does not exist in Form B. (Figure S17, B). The intensities of these two peaks also vary with the percentage of Form A.

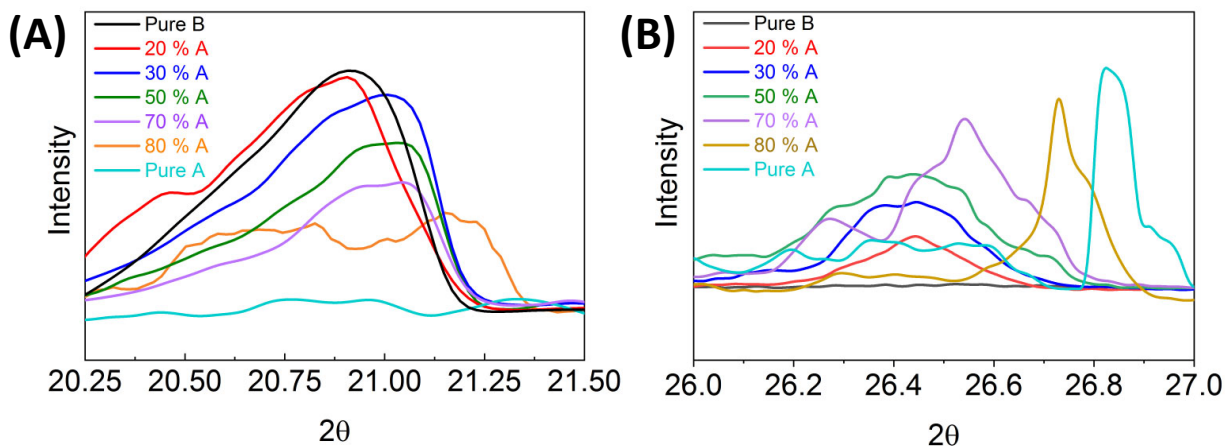


Figure S17: Variation in the intensity of characteristic peaks of (A) form B and (B) form A, with an increasing weight percentage of Form A.

Figure S17 A and B are magnified views from the selected peaks from Figure S16 and the target angle for the XRD measurement was from 8 to 28 degrees.

The measured relative intensities of these characteristic peaks (From Figure S17) fit a linear relationship with respect to the weight percentage of form A, as shown in Figure S18.

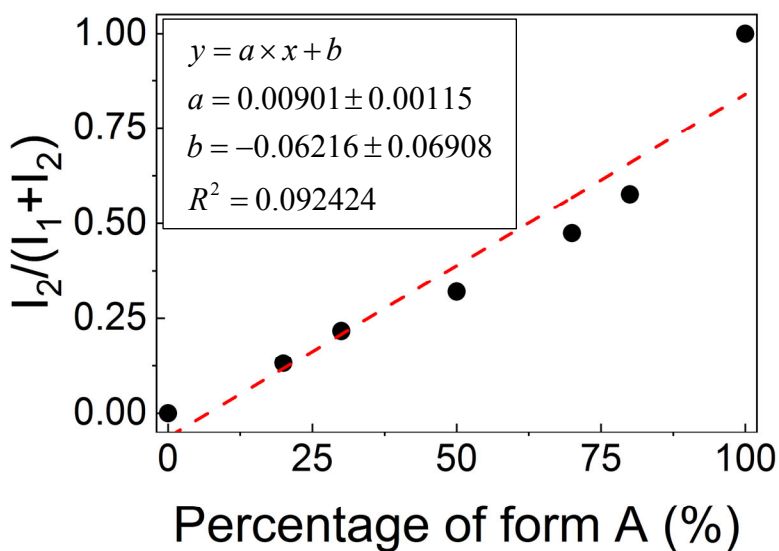


Figure S18: Calibration curve for the XRD spectra

Figure S18 relates the relative intensities of these two peaks in the samples to the percentage of each polymorph.

S8. Temperature Control Strategy for the Merged-Inlet Single-Well Device

In this study, all the experiments were performed at room temperature ($\sim 20^{\circ}\text{C}$). The antisolvent crystallization at room temperature does not need a temperature control platform. However, it is necessary to control the temperature precisely for cooling crystallization or antisolvent crystallization at higher temperatures. Here we introduce the idea for a jacketed merged inlet design where a coolant or heating fluid is recirculated around the mixer zone. In Figure S19, we have shown a 3D design of the jacketed microfluidic mixer.

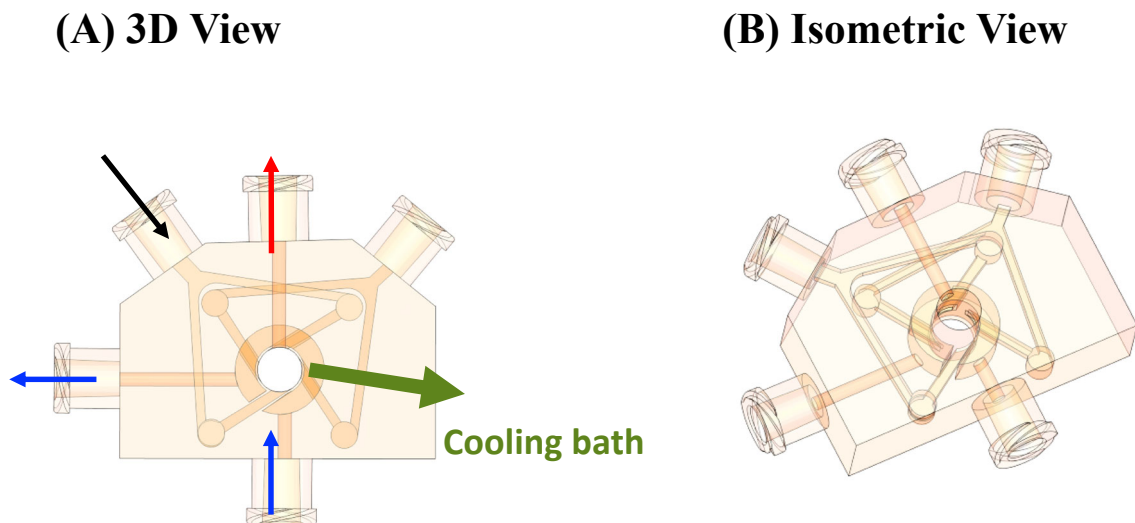


Figure S19: The 3D design of the jacketed microfluidic mixer (A) Top view, (B) Isometric view

S9. Increasing the Throughput of the Merged-Inlet Microfluidic Mixer.

The multi-well merged inlet device developed in this study has the potential to be used for the analysis of multiple experimental conditions in a single run. The number of experimental conditions or wells can be increased using the suggested design in Figure 1D of the main article. In Figure 1D, we have shown an array of the merged inlets with the hydraulic network, which combines the inlets of four wells and decreases the total number of inlets from eight to three. In Figure S20, we have extended this idea to show six series of hydraulic networks allowing up to 24 different experimental conditions to be evaluated in a single run. In principle, the limit on the maximum number of experimental conditions that can be evaluated in a single run will be determined by the resolution of the 3D printer and the overall size of the array of multi-well merged inlet devices.

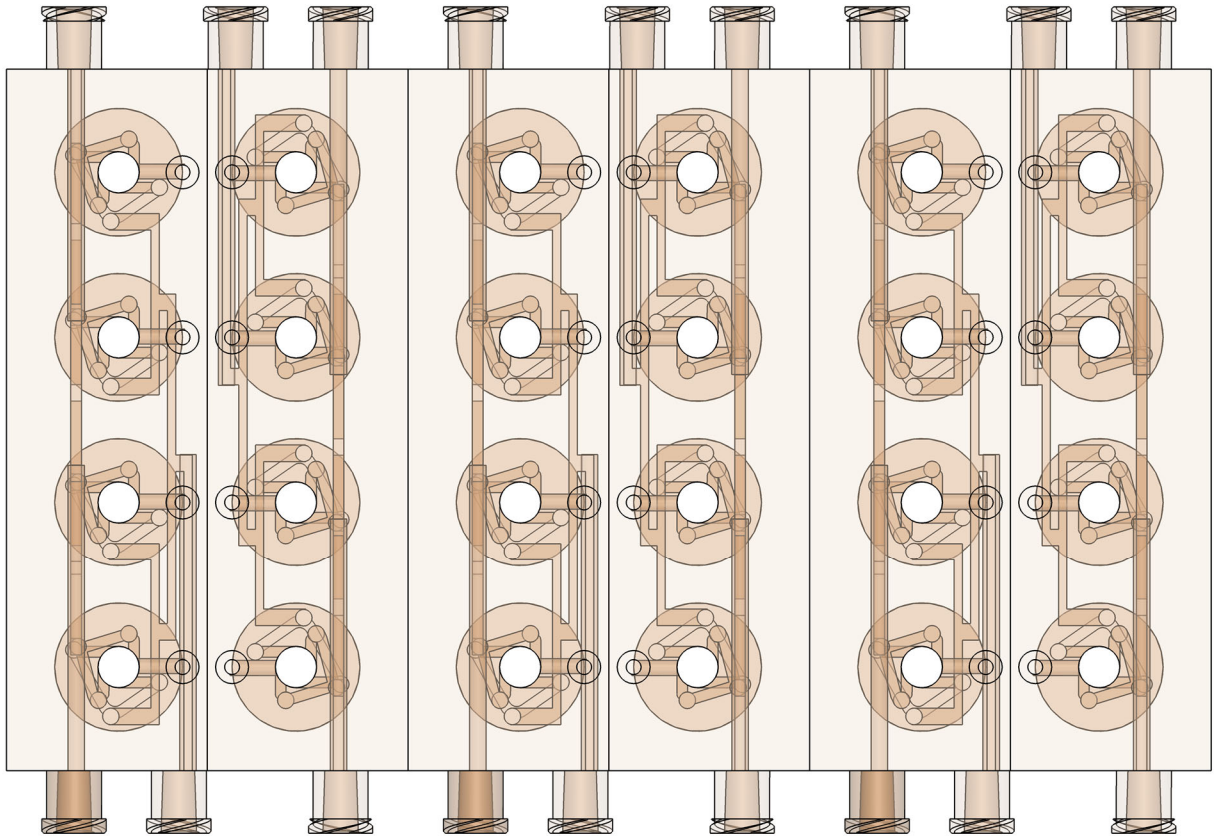


Figure S20: The top view of the 3D design for the six series of the hydraulic network arrays.